


Article

Experimental Study on Shear Mechanism of Rock-Like Material Containing a Single Non-Persistent Rough Joint

Sayedalireza Fereshtenejad ¹, Jineon Kim ² and Jae-Joon Song ^{1,*}¹ Department of Energy Resources Engineering, Research Institute of Energy and Resources, Seoul National University, Seoul 08826, Korea; a.r_fereshtenejad@snu.ac.kr² Department of Energy Resources Engineering, Seoul National University, Seoul 08826, Korea; kjineon@snu.ac.kr

* Correspondence: songjj@snu.ac.kr

Abstract: The geometrical and mechanical properties of non-persistent joints as well as the mechanical behavior of intact rock (rock bridges) are significantly effective in the shear strength of weakness planes containing non-persistent joints. Therefore, comprehensive knowledge of the shear mechanism of both joints and rock bridges is required to assess the shear strength of the planes. In this study, the shear behavior of specimens containing a single non-persistent rough joint is investigated. A novel procedure was used to prepare cast specimens embedding a non-persistent (disc-shaped) rough joint using 3D printing and casting technology, and the shear strength of the specimens was examined through an extensive direct shear testing program under constant normal load (CNL) condition. Three levels for three different variables of the joint roughness, rock bridge ratio, and normal stress were considered, and the effects of these factors on the shear behavior of prepared samples were tested. The experimental results show a clear influence of the three variables on the shear strength of the specimens. The results show that the normal stress applied to the jointed zone of weakness planes is considerable, and thus joint friction contribution should be taken into account during shear strength evaluation. Furthermore, the dilation mechanism of the specimens before and after failure was investigated through a digital image correlation analysis. Finally, a camcorder was used to analyze the location and sequence of the initiated cracks.

Keywords: shear behavior; non-persistent joint; rock bridge ratio; joint roughness; normal stress; digital image correlation



Citation: Fereshtenejad, S.; Kim, J.; Song, J.-J. Experimental Study on Shear Mechanism of Rock-Like Material Containing a Single Non-Persistent Rough Joint. *Energies* **2021**, *14*, 987. <https://doi.org/10.3390/en14040987>

Academic Editor:
Krzysztof Skrzypkowski

Received: 8 January 2021
Accepted: 9 February 2021
Published: 13 February 2021

Publisher's Note: MDPI stays neutral with regard to jurisdictional claims in published maps and institutional affiliations.



Copyright: © 2021 by the authors. Licensee MDPI, Basel, Switzerland. This article is an open access article distributed under the terms and conditions of the Creative Commons Attribution (CC BY) license (<https://creativecommons.org/licenses/by/4.0/>).

1. Introduction

When the engineering dimensions of an investigated site exceed the average joint size in the domain, the joints are surrounded by intact rock (rock bridge) in the rock mass and should be considered as non-persistent. Hence, joint size (persistence) should be precisely measured during the field survey owing to its substantial influence on the rock mass strength [1]. A combined shear plane where failure occurs is usually formed by the interaction of various non-persistent joints. Deng and Zhang [2] and Segall and Pollard [3] noted that the rupture of rock bridges connecting en-echelon joints may lead to the development of faults. In natural faults damage zones, en-echelon fractures, which occur as a unique set of sub parallel fractures, have often been found [4]. A comprehensive understanding of the spatial and geometrical properties of joints in a rock mass reveals various potential failure paths passing through the joints and rock bridges. Not only the bridges but also the joints have a significant effect on the shear behavior of the failure paths [5,6].

There has been considerable experimental and numerical research on the shear behavior of rough persistent rock joints from different points of view [7–29]. However, relatively few studies have investigated the shear mechanism of rock masses with non-persistent joints surrounded by intact rock. In previous experimental studies, edge-notched embedded joints were considered, and artificial materials were preferred to natural rocks for

creating specimens containing precise joint configurations with varying parameters. The spatial and geometric properties of joints in a rock mass (joint angle, rock bridge angle, joint size, rock bridge size, joint dispersion, length of overlap, and joint offset) as well as the boundary condition (normal load) and mechanical characteristics of the intact rock and joint surface (internal friction, internal cohesion, and joint friction) were systematically investigated [5,30–33]. In addition, to conduct a quantitative analysis which precisely detects the full failure mechanism of a rock mass with non-persistent joints, different numerical approaches such as the finite element method (FEM), discrete element method (DEM), and boundary element method (BEM), have been employed [31,34–39].

This study investigates the shear behavior of specimens with an embedded non-persistent rough joint using a direct shear test machine under constant normal load (CNL). The joint size/rock bridge ratio and the normal load as well as the joint roughness are the variables whose effects on the shear mechanism of the specimens are studied [40]. This research is different from previous studies for the following reasons.

- The applied specimen preparation techniques of previous studies resulted in specimens containing joints which are edge notched. Thin sheets were located within a casting frame prior to adding mortar and were removed as the mortar hardened. However, in this study, a novel method is applied to create non-persistent joints surrounded by intact material;
- In previous studies, the sheets applied to make joints caused a measurable aperture (gap) between the joint walls, corresponding to the thickness of the sheets. This gap prevents the contact between the joint walls, and consequently joint friction cannot be mobilized during shear process. However, using the casting approach applied in this study, the embedded joints are closed and joint friction is mobilized from the beginning of direct shear tests;
- In most previous experimental research on the shear behavior of rock masses, smooth non-persistent rock joints were modeled and analyzed. However, the specimen preparation procedure here allows one to create non-persistent close joints with different roughness levels along different directions.

2. Experimental Procedure

2.1. Equipment and Experimental Settings

A stiff servo-controlled direct shear test machine was used to perform all of the shear tests in this study (Table 1). Normal and shear displacements were measured using linear variable differential transformers (LVDTs), and strain gauge type load cells were applied to measure the shear loads. The load and displacement data were continuously recorded using a data acquisition system. The tests were conducted under constant normal load (CNL) condition by means of a hydraulic actuator. According to International Society for Rock Mechanics (ISRM) suggested methods, the normal load was continuously increased at a similar rate (0.01 MPa/s) up to the target normal stress (σ_n) [41]. The specimens were sheared up to 20 mm at the shear displacement rate of 0.2 mm/min. A 10 mm gap between the specimen holders was considered following the ISRM standard [41]. Moreover, fracture initiation moments were monitored using a camcorder at a frame rate of 30 fps (Figure 1b).

Table 1. Mechanical properties of 3DP and plaster specimens.

Material Type	UCS (MPa)	Tensile Strength (MPa)	Young's Modulus (GPa)	Poisson's Ratio	Basic Friction Angle (°)	Cohesion (MPa)	Internal Friction Angle (°)	Density (gr/cm ³)
3DP	15.9	2.4	6.16	—	41	—	—	—
Plaster	34	3.85	7.08	0.23	39.3	7.0	40	1.86

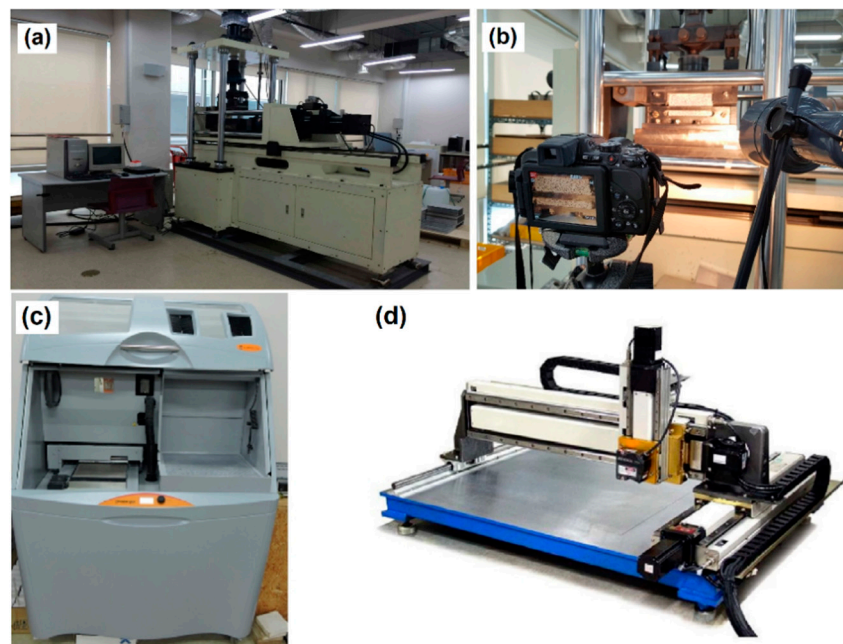


Figure 1. The equipment applied in this study; (a) Servo-controlled direct shear test machine, (b) Camera (Nikon, COOLPIX P600), (c) Zprinter[®] 450, (d) 3D laser profiler.

In the process of mold preparation to make rough joints, a powder-based 3D printer machine (Zprinter[®] 450) that uses binder jetting technology was used (Figure 1c). Comprehensive information about the functionality of the 3D printer and its applicability to rock mechanics is available in the authors' previous study [42]. In addition, a 3D laser profiler was applied to measure the surface roughness of the 3D printed (3DP) molds, the silicone molds, and the plaster joints applied in this study (Figure 1d). The 3D laser profiler determines the roughness parameter by digitizing the surface of a joint using a laser displacement meter (Kenyence LK-G150). This profiler is composed of a laser displacement meter, a motion control system, and a LabVIEW computer which controls the entire system and exports the measured data. The motion control system (Jeongwon Mechatronics) controls the position of the laser displacement meter using servo-motors which are placed on the x , y , and z axes.

2.2. Materials

An industrial gypsum powder was mixed with water at a mass ratio of 3:1 to create the mortar required to cast plaster specimens. The powder consists of more than 99% bassanite. Three NX-size plaster specimens with a height of 130 mm and three more with a height of 65 mm were prepared. Three uniaxial compressive strength (UCS) tests and three Brazilian tests were carried out on the prepared specimens using MTS 816 system to measure the UCS, Young's modulus, and tensile strength according to the ISRM suggested methods [43]. Moreover, three direct shear tests at different normal stresses of 1 MPa, 1.5 MPa, and 2 MPa were carried out to measure the basic friction angle of the plaster specimens. Table 1 lists the mechanical properties of plaster specimens. VisiJet PXL Core powder and VisiJet[®] PXLTM Clear binder were used to make 3DP molds. A printing layer thickness of 0.089 mm and a binder saturation level of 120% were selected to print these specimens. Some of the mechanical characteristics of the 3DP molds are listed in Table 1. To create the silicone molds to cast the plaster rough joints, two types of silicone (Molkang), one with viscosity of 6000 MPa·s (Moldmaster (Soft)) and the other one with viscosity of 16,000 MPa·s (Moldmaster (Normal)) were applied.

2.3. Variables and Levels

This study investigates the effects of three variables (rock bridge ratio (ζ), normal stress (σ_n), and joint roughness (Z_2)) on the shear behavior of plaster specimens with a single non-persistent joint. Z_2 (the root mean square of the first derivative of the profile) is a commonly used statistical parameter applied in this study to quantify the roughness of joint profiles [44]. The roughness levels selected in this study, low (LR), medium (MR), and high (HR), almost cover a wide range of joint roughness in nature. Here, the rock bridge ratio (ζ) is defined as the ratio of the bridged area to the weakness plane area. As listed in Table 2, three different levels were selected for each factor. As the loading capacity of the applied direct shear test machine in shear direction was limited, 2 MPa was selected as the maximum value of the normal stress. The normal stress condition of this study is similar to the condition that exists at shallow depth. This normal stress condition was frequently selected in previous studies [20,23,45].

Table 2. Selected levels for the factors affecting the shear behavior of specimens with a non-persistent rough joint.

Factors (Variables)	Levels		
	1	2	3
Joint roughness	JRC = 6.6 Smooth, nearly planar	JRC = 11.7 Smooth undulating	JRC = 17.6 Rough undulating
Rock bridge ratio (ζ)/Joint size (mm)	0.71/80	0.59/95	0.45/110
Normal stress (MPa)	1	1.5	2

2.4. Specimen Preparation Procedure

2.4.1. Rough Joint Specimens (J Specimens)

Three different levels of roughness, denoted here as low, medium, and high, were selected to make 27 disc-shaped joint specimens to investigate the shear behavior of disc-shaped rough joints of three sizes under three different normal stress levels. Nine different surfaces for a combination of two factors (joint size, joint roughness) at three levels were required. To make rough plaster joints, nine silicone molds were created using the following procedure. First, a Matlab script was used to generate isotropic artificial rough surfaces with the given parameters (root mean square roughness, fractal dimension, size, and resolution) in the point cloud data format [46]. The code is based on simulating the surface topography/roughness by means of fractals. It uses the Fourier concept (specifically the power spectral density) for surface generation. Afterwards, the point cloud data files were converted to the STL format, and the STL files were then modified and 3D printed. Oil-based paint was uniformly sprayed onto rough surfaces of the 3DP molds for easily release from the final silicone molds (Figure 2a). Finally, to cast the final disc-shaped silicone molds, the 3DP molds were placed in steel molds located on a leveling table. A 10 mm layer of a durable silicone with relatively high viscosity was poured onto the rough surface of the 3DP molds, and a thinner layer (5 mm) of low viscosity silicone was poured onto the cured first layer to make a smooth and flat bottom (Figure 2b). Each plaster cylinder with a rough surface made by applying the silicone and steel molds (Figure 2c) was then encapsulated in the same casting material with a higher gypsum powder to water ratio (3.55:1) to be secured in each half of the specimen holder (Figure 2d).

All of the plaster disc-shaped joints were cast using these nine silicone molds. However, the roughness of the generated surface in Matlab gradually degraded during the molding process. As the final goal was to create three plaster joints of various sizes (three sizes) with the same roughness, continuous attempts to generate rough surfaces (by Matlab) were made until the final goal was reached. The roughness value of each joint was measured considering several sampling profiles parallel to the shear direction. The distance

between two adjacent sampling profiles was set to be 0.5 mm. As the applied roughness parameter (Z_2) is sensitive to the sampling interval [47], the same sampling interval of 0.5 mm was considered along each sampling profile. The number of points sampled for 80, 95, and 110 mm joints were 7338, 10,336, and 13,882, respectively. Z_2 values of the sampling profiles were measured for each joint, and the average value was eventually considered as the representative roughness value for the joint. Table 3 lists the measured Z_2 values of the generated, 3DP, and final plaster joint surfaces for all nine cases. The converted JRC values in the table were calculated using the equation proposed by Tse and Cruden ($JRC = 32.2 + 32.47 \log Z_2$) [44]. Figure 3 illustrates the surfaces of the final plaster joints scanned by a 3D laser profiler.



Figure 2. Preparation procedure of joint specimens; (a) 3DP mold, (b) silicone mold, (c) plaster rough joint, (d) encapsulated joint.

Table 3. Roughness properties of generated, 3DP, and final plaster joint surfaces.

Joint Diameter (mm)	Roughness Level	Roughness Value (Z_2)		
		Generated Surface	3DP Joint	Final Plaster Joint
80	Low (LR)	0.268	0.162	0.163 (Converted JRC = 6.62)
	Medium (MR)	0.390	0.238	0.235 (Converted JRC = 11.78)
	High (HR)	0.659	0.365	0.354 (Converted JRC = 17.56)
95	Low (LR)	0.267	0.161	0.163 (Converted JRC = 6.62)
	Medium (MR)	0.460	0.238	0.234 (Converted JRC = 11.72)
	High (HR)	0.675	0.364	0.356 (Converted JRC = 17.64)
110	Low (LR)	0.267	0.161	0.163 (Converted JRC = 6.62)
	Medium (MR)	0.435	0.239	0.232 (Converted JRC = 11.6)
	High (HR)	0.693	0.364	0.358 (Converted JRC = 17.71)

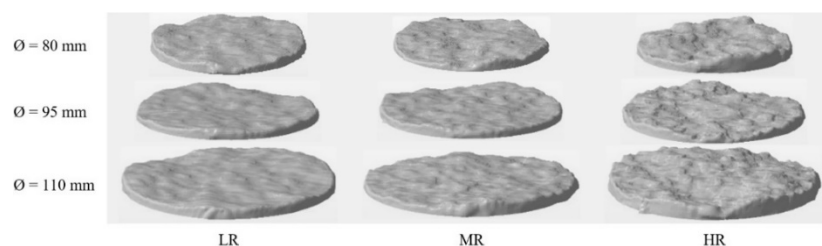


Figure 3. Surfaces of final plaster joints at three levels of roughness.

2.4.2. Specimens Containing a Single Non-Persistent Open Joint (Br specimens)

Several rectangular cuboid plaster specimens (length: 150 mm, width: 115 mm, height: 130 mm) with a single non-persistent open joint were cast to investigate the shear behavior of rock bridge. The preparation process of Br specimens is illustrated in Figure 4a. A detailed explanation about the sample preparation process of Br specimens is explained in the authors' previous study [48].

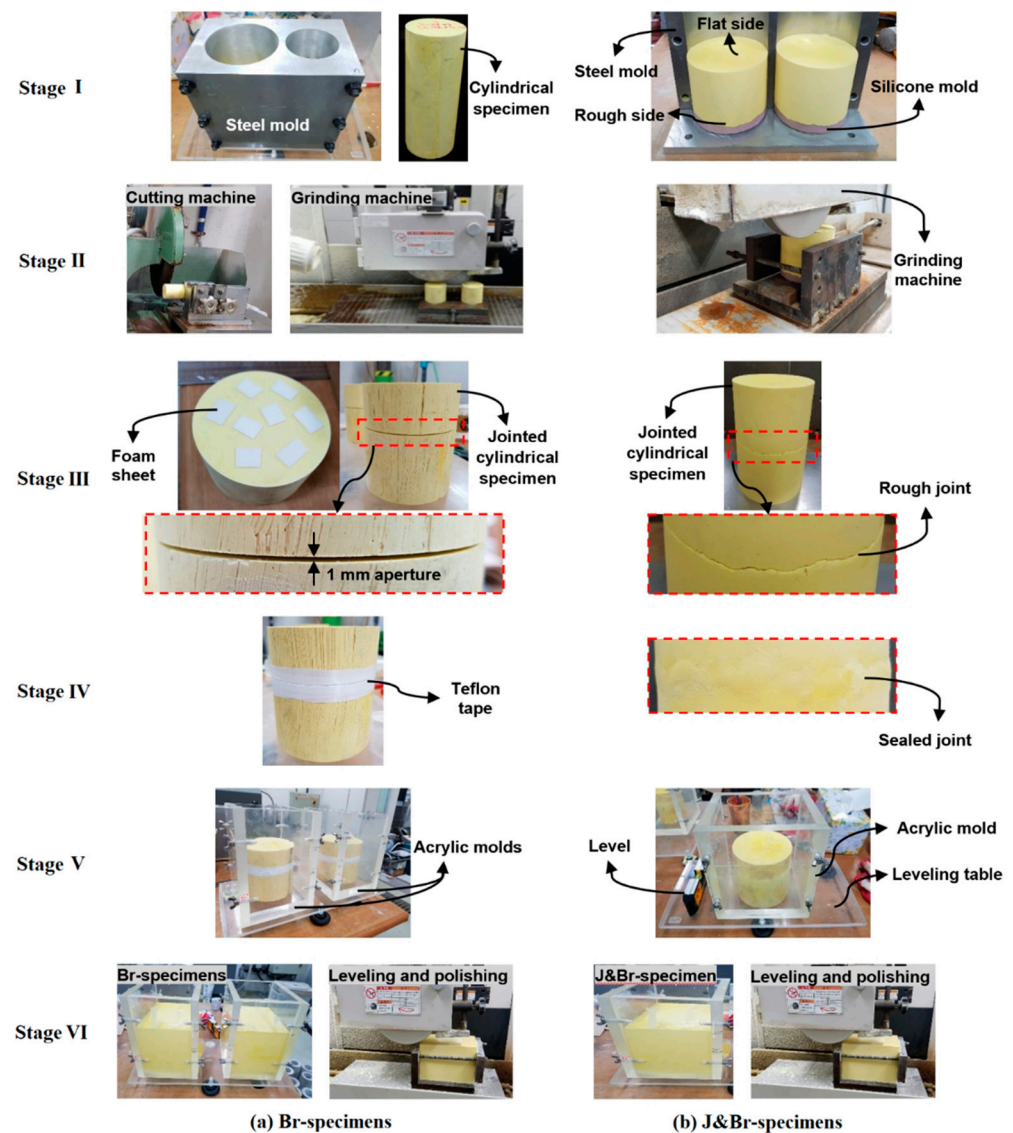


Figure 4. Step-by-step preparation process of (a) Br specimens and (b) J&Br specimens.

2.4.3. Specimens Containing a Single Non-Persistent Rough Joint (J&Br specimens)

Twenty-seven rectangular cuboid plaster specimens (length: 150 mm, width: 115 mm, height: 130 mm) embedding a single non-persistent rough joint were cast to investigate the simultaneous shear behavior of joint and rock bridge. The specimen preparation process of J&Br specimens is quite similar to that applied for the Br specimens and consists of the following stages (Figure 4b).

1. Two cylindrical plaster specimens each of which has one rough side and one flat side are initially cast using a steel mold and a pair of silicone molds. The rough sides of the cylindrical specimens represent the upper and lower walls of a joint;
2. The other side of each cylindrical specimen (flat side) is smoothed by a grinding machine;
3. The rough sides of the prepared cylindrical specimens are placed on each other to make a cylindrical specimen containing an interlocked rough joint in the middle;
4. To prevent the seepage of plaster mortar into the rough joint, the joint is plastered around the circumference with a very thin layer of slightly cured and sticky mortar;
5. The cylinder with a sealed rough joint is then put in a hexahedron acrylic mold which is placed on a leveling table;
6. The space around the jointed cylinder is filled with plaster mortar, and the sides of the cured specimen are leveled and smoothed utilizing a grinding machine.

The preparation process of one Br specimen or one J&Br specimen requires around eight hours. All of the specimens were tested seven days after the preparation process, during which they were kept at room temperature. As mentioned above, the casting process of Br specimens and J&Br specimens consists of two main steps. First, a jointed cylindrical part is cast, and once it solidifies, the surrounding rock bridge part is cast. Therefore, this inevitable interruption during the casting process may cause a weak surface around the cylindrical specimen. To investigate the possible effect of these weak surfaces on the results, all the specimens made for this study were carefully observed during and after the experiments. No crack was found to be initiated from or propagated toward those weak surfaces. Therefore, the experimental results of this study were not affected by the weak surfaces created during the specimen preparation process. It is important to note that the tensile resistance of the applied Teflon tape is insignificant under small deformations, hence it provides no resistance against the normal and shear deformation of open joints in Br specimens.

3. Experimental Results

The simultaneous contributions of the friction mobilized by the joint and the cohesion of the rock bridge to the shear resistance of weakness planes with non-persistent joints are highly complex. Finding the distribution of the applied normal load on jointed and bridged zones is a key factor to determine the shear strength of the planes. In some previous analytical studies [49], the normal stresses distributed on the jointed and bridged zones of a weakness plane were assumed to be identical and equal to the nominal normal stress (average normal stress applied to the entire area of the weakness plane), $\sigma_n^{nominal}$. In previous experimental research, the load was only applied to the bridged zone of weakness planes due to applied specimen preparation procedures; as a result, the joint roughness contribution to the shear strength was inconsiderable. As the normal stiffness of the rock bridge, K_n^{Br} , and the normal stiffness of the embedded joint, K_n^J , typically differ, the amount of normal load applied on each zone is proportional not only to its area on the weakness plane but also to its normal stiffness. Knowing the normal stiffness of the joint and rock bridge determines the amount of normal load distributed on the jointed and bridged zones of a weakness plane when only the normal load is applied. However, it provides no precise information about the normal stress distribution regime when both normal and shear loads are applied (direct shear test condition). Therefore, determination of normal stresses on the jointed and bridged zones of weakness planes (σ_n^J and σ_n^{Br}) subjected to the direct shear test is very complicated. The experimental strategy of this study is adopted to investigate the normal load distribution regime and the effects of joint roughness, normal load, and rock bridge ratio on the shear behavior of rock mass embedding a joint, and is categorized into two cases. Below, the experimental results obtained for each case are reported.

3.1. Case I

In case I experiments, the applied normal load (N_L) is entirely distributed over the bridged zone of the weakness plane (A_{Br}). Therefore, the normal stress applied onto the bridged zone is higher than the nominal normal stress ($\sigma_n^J = 0$, $\sigma_n^{Br} = \frac{N_L}{A_{Br}} > \sigma_n^{nominal}$), and the shear strength of the specimen is solely dominated by the shear resistance of the rock bridge. Several Br specimens containing a single joint of three different sizes ($\varnothing = 80$ mm, $\varnothing = 95$ mm, and $\varnothing = 110$ mm) were prepared and subjected to direct shear tests under three different normal stress levels (1, 1.5, and 2 MPa). As the joints are open, the shear test results reflect only the resistance of the bridged zone of the weakness planes. Figure 5 shows the shear tests results. As expected, the shear strength is higher for the cases with greater rock bridge ratios subjected to higher normal stresses. The values of the peak shear displacement and peak dilation for the tested samples are illustrated in Figure 6a,b, respectively. As shown, the specimens with greater rock bridge ratios subjected to higher normal stresses were sheared for longer distances before failure, and those with greater

rock bridge ratios subjected to lower normal stresses experienced more dilation at the failure moment.

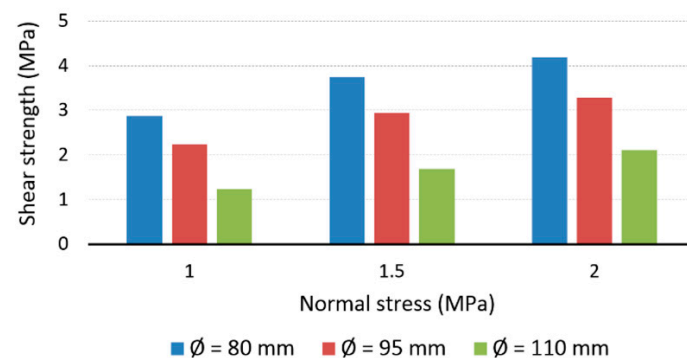


Figure 5. Shear strength of Br specimens (case I: $\sigma_n^J = 0$).

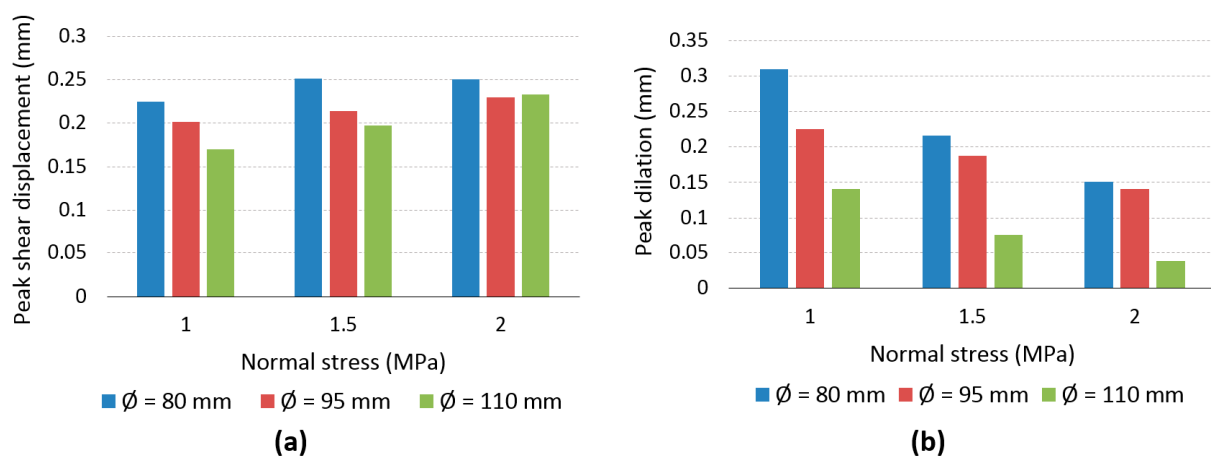


Figure 6. (a) Peak shear displacement and (b) peak dilation values for Br specimens subjected to direct shear test condition (case I: $\sigma_n^J = 0$).

3.2. Case II

In this section, the experimental results of direct shear tests carried out on J&Br specimens are provided. These results reflect a complicated mechanism when a weakness plane is under direct shear test condition with the shear resistance depending on the simultaneous mobilization of joint friction and intact rock cohesion. Figure 7 shows the shear strength of the J&Br specimens with a single embedded joint of three different sizes ($\varnothing = 80$ mm, $\varnothing = 95$ mm, and $\varnothing = 110$ mm) and three different roughness levels (LR, MR, and HR) when subjected to three normal stress levels (1, 1.5, 2 MPa). As shown in the figure, the normal stress and rock bridge ratio have strong effects on the shear strength of the J&Br specimens. The shear strength of the specimens increases by when the rock bridge ratio and applied normal stress increase. Although the overall trend shows a direct relationship between the joint roughness and the shear strength of J&Br specimens, the effect of the joint roughness on the shear strength is less than that of rock bridge ratio or normal stress. Figures 8 and 9 depict the peak shear displacement and peak dilation of the J&Br specimens, respectively. The overall results show that the specimens with greater rock bridge ratios experienced greater peak shear displacement when undergoing greater normal stresses (Figure 8). Figure 9 indicates that J&Br specimens with greater rock bridge ratios experienced greater peak dilation when undergoing lower normal stresses.

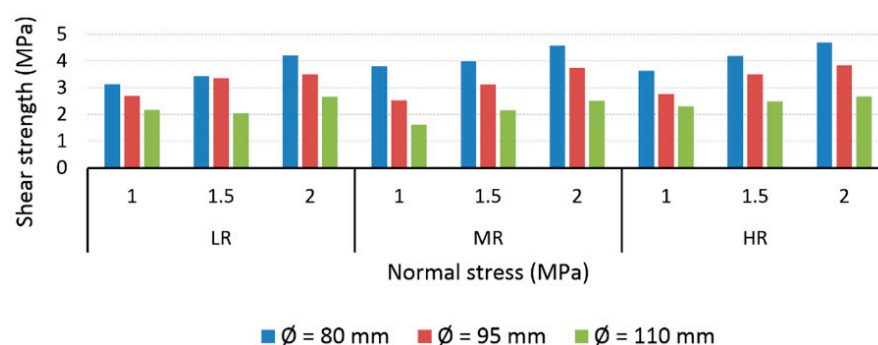


Figure 7. Shear strength of J&Br specimens embedding single joint with different sizes and roughness under different normal stress levels.

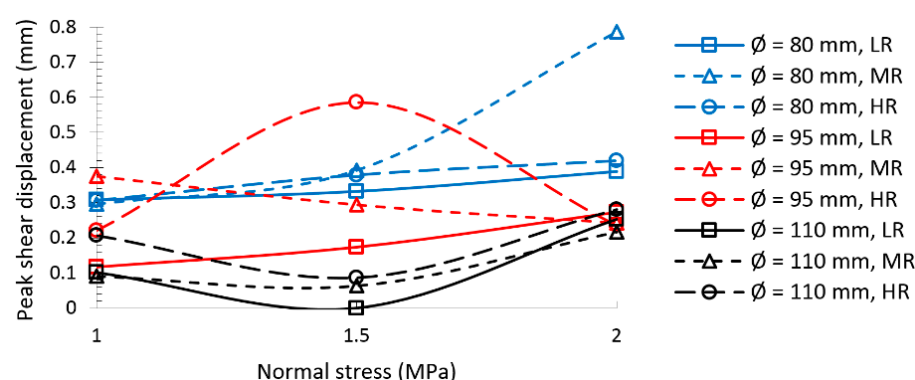


Figure 8. Peak shear displacement of J&Br specimens embedding a single joint with different sizes and roughness under different normal stress levels.

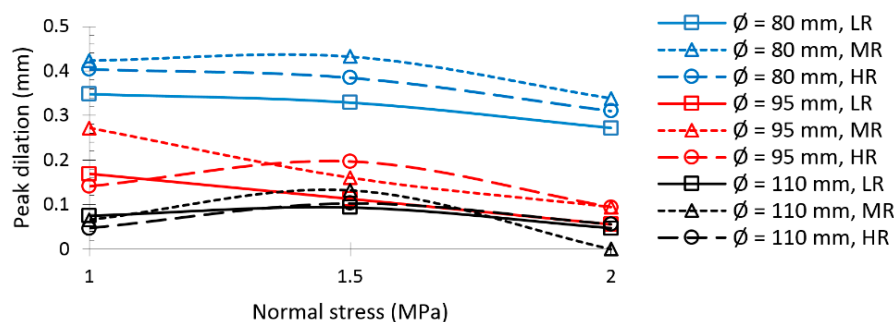


Figure 9. Peak dilation of J&Br specimens embedding a single joint with different sizes and roughness under different normal stress levels.

Five J&Br specimens were subjected to uniaxial compressive loading to study the effects of rock bridge ratio and joint roughness on the normal stiffness. Figure 10 shows the normal stress-normal deformation curves of the J&Br specimens. The results clearly demonstrate that the normal stiffness varies with the normal stress in the initial non-linear stage and remains constant afterwards. The non-linear stage implies the closure behavior of the embedded joint under uniaxial loading and the subsequent linear stage denotes the normal deformation of J&Br specimens when the embedded joint is closed [50]. The linear stage in fact shows the normal deformation of an intact sample subjected to uniaxial loading, hence the curves in this stage are almost parallel. As shown, the normal deformation is greater for the J&Br specimens with wider joints. The normal stress-normal deformation curves of the J&Br specimens embedding a 95 mm diameter joint show that the roughness of embedded joint has no systematic effect on the normal deformation of J&Br specimens subjected to uniaxial compressive loading. The shear stiffness of the

J&Br specimens subjected to direct shear test condition were investigated from their shear stress–shear displacement curves. The shear stiffness values were measured from the linear part of the curves before the peak shear stress (Table 4). The results show that rock bridge ratio, normal stress, and roughness of embedded joints have no systematic effect on the shear stiffness of the J&Br specimens. The residual shear strength of the J&Br specimens was also measured from the shear stress–shear displacement curves (Table 4). The results clearly show that the residual shear strength is greater when J&Br specimens are subjected to greater normal stress levels. In most of the cases, the residual shear strength is greater for the J&Br specimens embedding a rougher joint. The effect of roughness on the residual shear strength is more pronounced when the rock bridge ratio of J&Br specimens is smaller. Moreover, the values of cohesion and friction angle of J&Br specimens are provided in Table 4. The results show that the cohesion increases when the rock bridge ratio is increased. Neither Rock bridge ratio nor joint roughness has a systematic effect on the friction angle of J&Br specimens.

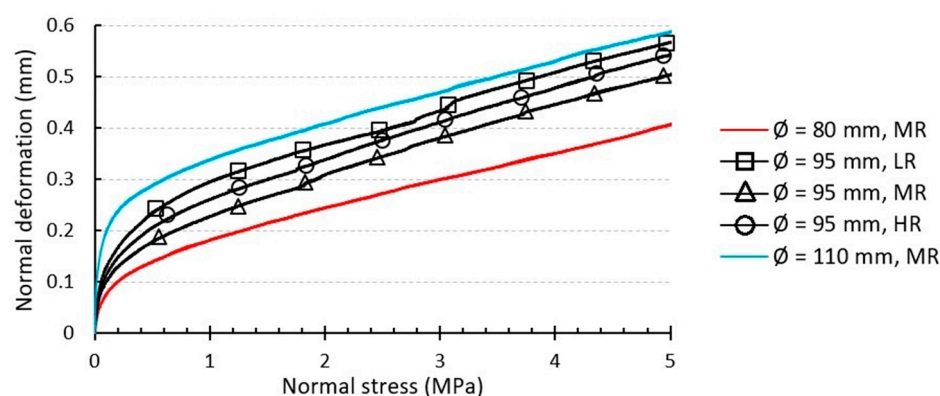


Figure 10. Normal stress-normal deformation curves of J&Br specimens subjected to uniaxial compressive loading.

Table 4. Shear stiffness and residual shear strength of J&Br specimens subjected to direct shear test condition.

Joint Diameter (mm)	Roughness Level	Shear Stiffness (MPa/mm)			Residual Shear Strength (MPa)			Cohesion (MPa)	Friction Angle (°)
		σ_n (MPa)	1	1.5	2	1	1.5	2	
80	LR	7.09	11.47	15.5	1.59	1.74	2.21	1.98	47.1
	MR	14.83	9.42	7.69	1.67	1.85	2.17	2.96	37.9
	HR	16.11	12.8	13.62	1.56	1.99	2.1	2.58	46.7
95	LR	25.19	24.24	7.05	1.44	1.75	2.39	1.98	38.9
	MR	8.57	13.21	10.8	1.51	1.8	2.4	1.3	50.7
	HR	12.16	10.75	15.07	1.7	2.22	2.67	1.75	47.3
110	LR	7.66	6.56	8.97	1.43	1.75	2.16	1.57	25.8
	MR	15.48	9.5	12.44	1.52	1.84	2.36	0.76	41.7
	HR	8.51	12.7	8.44	1.72	2	2.68	1.95	20.0

4. Discussion

4.1. Joint Friction Contribution

The actual shear mechanism of the specimens with a non-persistent rough joint and the true physical interaction between the bridged and jointed zones of the weakness plane during shearing process occur for the case II experiments. Hence, the shear strength of the specimens obtained from the experiments of case I was compared to those obtained from the case II experiments. Figure 11a–c show the shear strengths obtained from case I and case II experiments when the joint diameters are 80 mm, 95 mm, and 110 mm,

respectively. The comparison clearly shows that the maximum shear load required to break J&Br specimens is underestimated when the friction contribution of the jointed zone is ignored. The difference between the shear strength obtained from case I and case II experiments (subtracting the values of the red bars from those of the blue bars in Figure 11) is illustrated in Figure 12. As shown in most of the cases, the greater differential shear strength is for the specimens with wider joints. This shows that the involvement of the embedded joint in the shear strength is more pronounced when a wider portion of the plane of weakness is discontinuous. The normal stress and the joint roughness do not appear to have any constant influence on the differential shear strength. Overall, the results of experiments show that the portion of applied normal load distributed to the jointed zone of weakness plane is not negligible and therefore joint friction contribution should be considered when evaluating the shear strength of the planes.

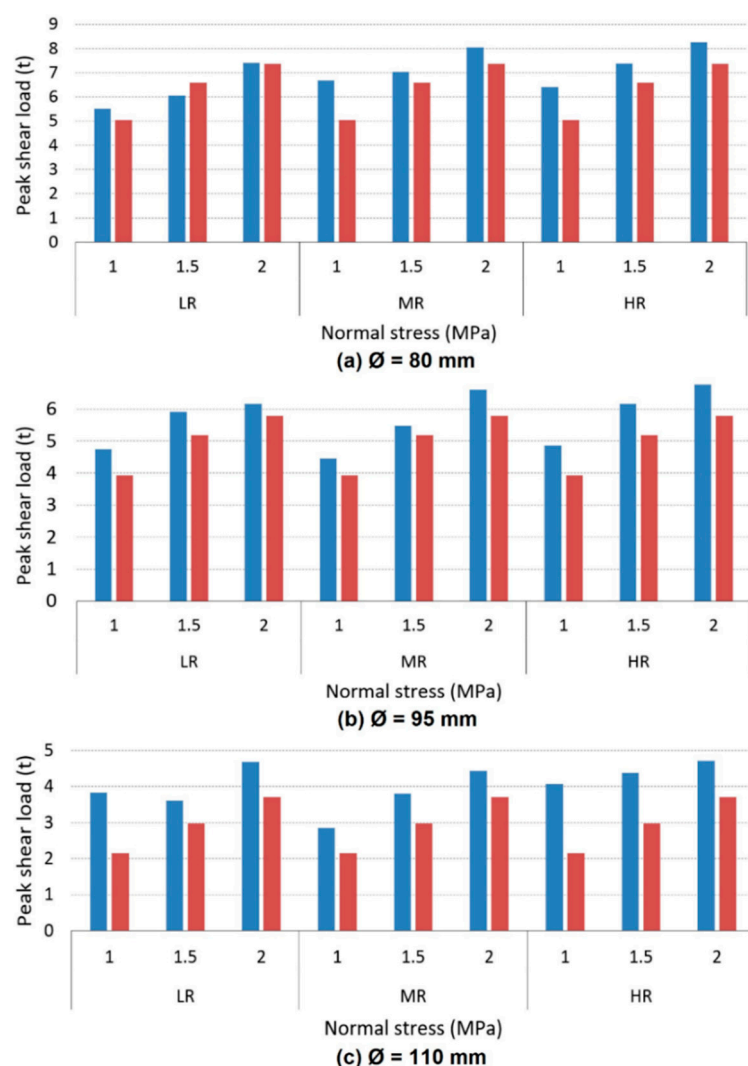


Figure 11. Comparison of the shear strength of the specimens containing a non-persistent rough joint obtained from case II experiments (blue bars) with the ones from case I experiments (red bars) when the joint diameter is (a) 80, (b) 95, and (c) 110 mm.

Joint friction mobilization is another significant factor in the evaluation of the shear strength of weakness planes. A total of 27 J specimens with three different joint sizes ($\varnothing = 80$ mm, $\varnothing = 95$ mm, and $\varnothing = 110$ mm) and three different roughness (LR, MR, and HR) were prepared and subjected to direct shear tests under three different normal stress levels (1, 1.5, and 2 MPa). Figure 13 illustrates the peak shear displacements of J specimens and those of J&Br specimens. As shown, the shear displacement required for J specimens

to reach their ultimate shear strength is much greater than the peak shear displacement of the J&Br specimens. This means that the friction of jointed zone of J&Br specimens is partially mobilized at the moment of failure. Moreover, the results of Figure 13 show that the peak shear displacement of J&Br specimens is less than 1 mm. As mentioned, previous specimen preparation technique (application of rough sheets with 1 mm thickness to make non-persistent joints) limits us to make joints with a certain amount of aperture. As the peak shear displacement of the J&Br specimens is smaller than the horizontal gap between the joint walls, joint friction is not mobilized at failure moment. Therefore, the proposed specimen preparation procedure of this study is suggested to investigate the shear behavior of specimens with non-persistent joints, knowing that the friction contribution of embedded joints is considerable.

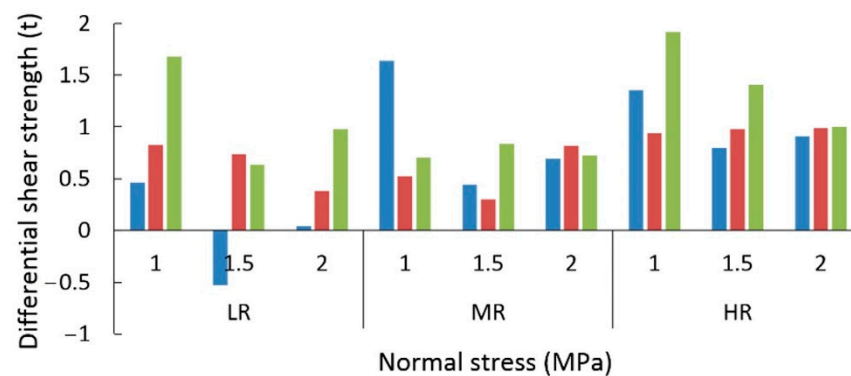


Figure 12. The difference between peak shear loads obtained from case I and case II experiments.

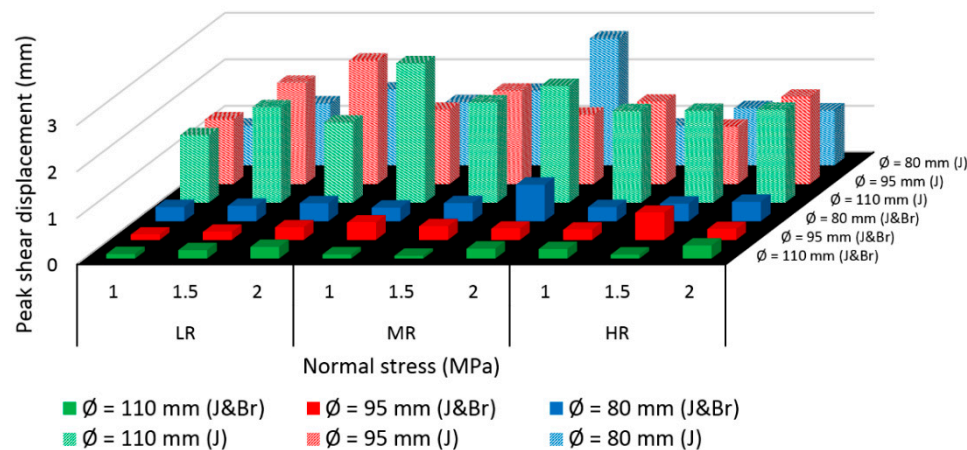


Figure 13. Comparison of peak shear displacements of J and J&Br specimens.

4.2. Dilation Mechanism

Figure 14 shows the shear stress/dilation-shear displacement curves of the J&Br specimens subjected to the direct shear test condition. As shown in the figure, the dilation curves consist of three phases. The first represents the dilation of the specimens before the moment of failure. This phase begins with the initiation of the test and ends at the point corresponding to the peak shear stress, denoted by the dash-dotted line arrows in Figure 14. In the first phase, all of the J&Br specimens experienced a certain amount of dilation, mostly controlled by the normal load applied to them. The shear stress drops sharply at the moment of failure and reaches a certain point (toe). The second phase of dilation starts at the point corresponding to the peak shear stress and ceases at the point corresponding to the toe, denoted by the dashed line arrows. In this phase, the specimens dilate due to crack propagation and coalescence. This dilation is followed by compression

for some specimens (e.g., $\varnothing = 95$ mm, MR, 2 MPa) because the cracks are closed after coalescence. The third phase starts immediately after the second phase and expresses the dilation behavior of the failure planes created after the specimens were broken into two halves in the second phase. The experimental results show that the specimens subjected to higher normal stresses underwent less amount of dilation, and those with rougher and smaller joints experienced a greater amount of dilation during the last phase of dilation.

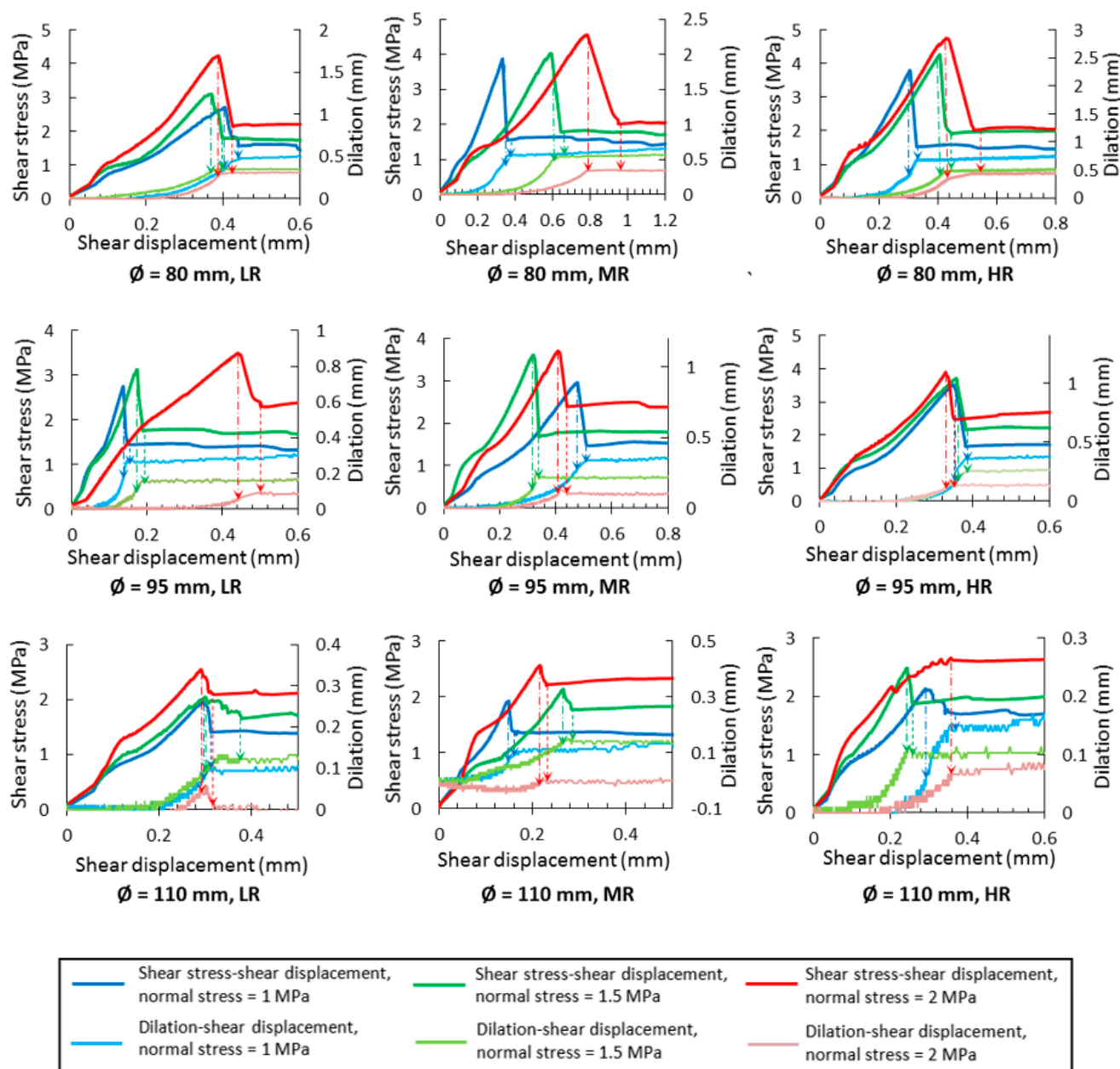


Figure 14. Dilation mechanism of J&Br specimens considering their shear stress–shear displacement curves.

The rough jointed zone of the weakness planes causes dilation to a very limited extent while a J&Br specimen is sheared. However, a large portion of the peak dilation of the J&Br specimens (Figure 9) is expected to be caused by torque exerted due to the existing gap between the specimen holders. To investigate the cause of the dilation, the displacement field on one J&Br specimen ($\varnothing = 95$ mm, HLR, 2 MPa) was analyzed using the DIC technique. Figure 15a illustrates the specimen on which some points whose vertical displacements are desired are marked. The central line in the figure depicts the intersection

of the shear plane where the joint is located and the outer boundary of the specimen. The vertical displacements of ten points located at the top, center, and bottom of the specimen were investigated (Figure 15a). Figure 15b illustrates the vertical displacements of the points before the failure of the specimen. As shown in this figure, the vertical displacements of the points on the right side of the specimen (Tr, Cr, and Br) are greater than those on the middle (Tm, Tm1, Cm, and Bm), and the vertical displacements of the points on the middle are greater than those on the left side (Tl, Cl, and Bl). This information simply reveals the rotation of the specimen along the axis of rotation, and this rotation causes dilation during the shear test. The points located on the top, center, and bottom parts of the left/right side of the specimen had similar upward displacements (Tl, Cl, and Bl or Tr, Cr, and Br). However, the points located at the middle-top (Tm and Tm1) zone were displaced slightly more than those located at the middle-center (Cm) and middle-bottom (Bm) zones. This relative vertical displacement at the middle of the specimen reflects the initiation of a crack which propagated between Cm and Tm1.

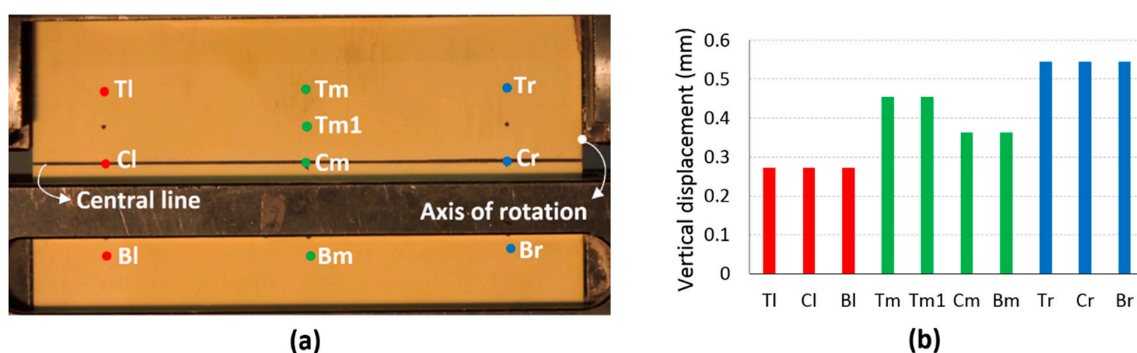


Figure 15. (a) The location of the points selected for DIC analysis, (b) Upward displacement of the points.

4.3. Cracking Analysis

In most previous experimental and numerical studies of the failure mechanisms of specimens containing edge-notched non-persistent (open) joints under direct shear test condition, the tensile mode was more frequently reported as the cause of the initiation and propagation of cracks inside a rock bridge [5,30,31,35,39]. All of the J&Br specimens were monitored using a camcorder while they were subjected to the direct shear test condition, and the cracking process was studied extensively. Figure 16 indicates that the shear load is applied to the lower part of the specimens from the left side and that the normal load is exerted downward over them. The vertical movement of lower shear box is restricted and the upper shear box is only allowed to move vertically. As shown in the figure, cracks initiate and propagate from three different zones: the left side, the center, and the right side of the specimens.

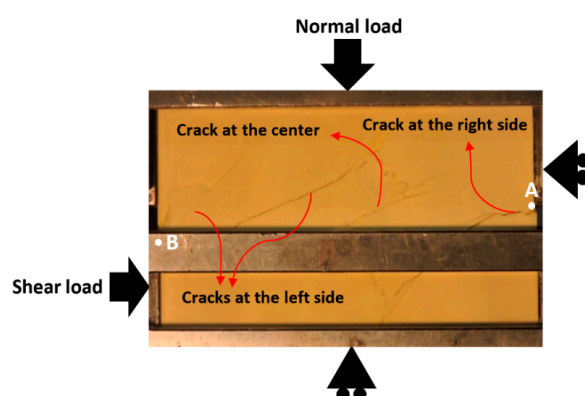


Figure 16. Crack initiation and propagation zones in J&Br specimens under direct shear test condition.

Figure 17 shows the initiation moment and the sequence of cracks on the shear stress–shear displacement curves (by the \times , $+$, and \circ symbols) leading to the failure of J&Br specimens subjected to the direct shear test condition. The sequence of initiation of cracks is indicated in the legends of the graphs in Figure 17. The locations of cracks which initiated at the same time are indicated in parentheses, and the star symbol beside a cracking zone indicates that the crack initiated and propagated explosively through the zone. As shown, the first crack initiated in the vicinity of point A (the axis of rotation) and propagated toward the circumference of the embedded joint and then to the lower part of the specimen. For the cases with smaller joints ($\varnothing = 80$ mm), the first cracks most commonly initiated at the center of the specimens. The first cracks most commonly initiated before the failure of the specimens and did not have any significant impact on the path of the shear stress–shear displacement curves. The cracks which initiated at the central zone did not affect the curves. Finally, the last crack, connecting the left side of the joint circumference to point B, eventually results in a rupture with the embedded joint and the right-side crack. The final cracks always coincide with the peak shear stress and dramatically reduce the shear resistance of the specimens. The J&Br specimens with greater rock bridge ratios ($\varnothing = 80$ mm and $\varnothing = 95$ mm) mostly experienced an explosive and violent rupture. However, the final cracks propagated smoothly through the specimens containing a wider joint ($\varnothing = 110$ mm). The normal stress and joint roughness have no clear effects on the crack initiation moment and the sequence of the cracks.

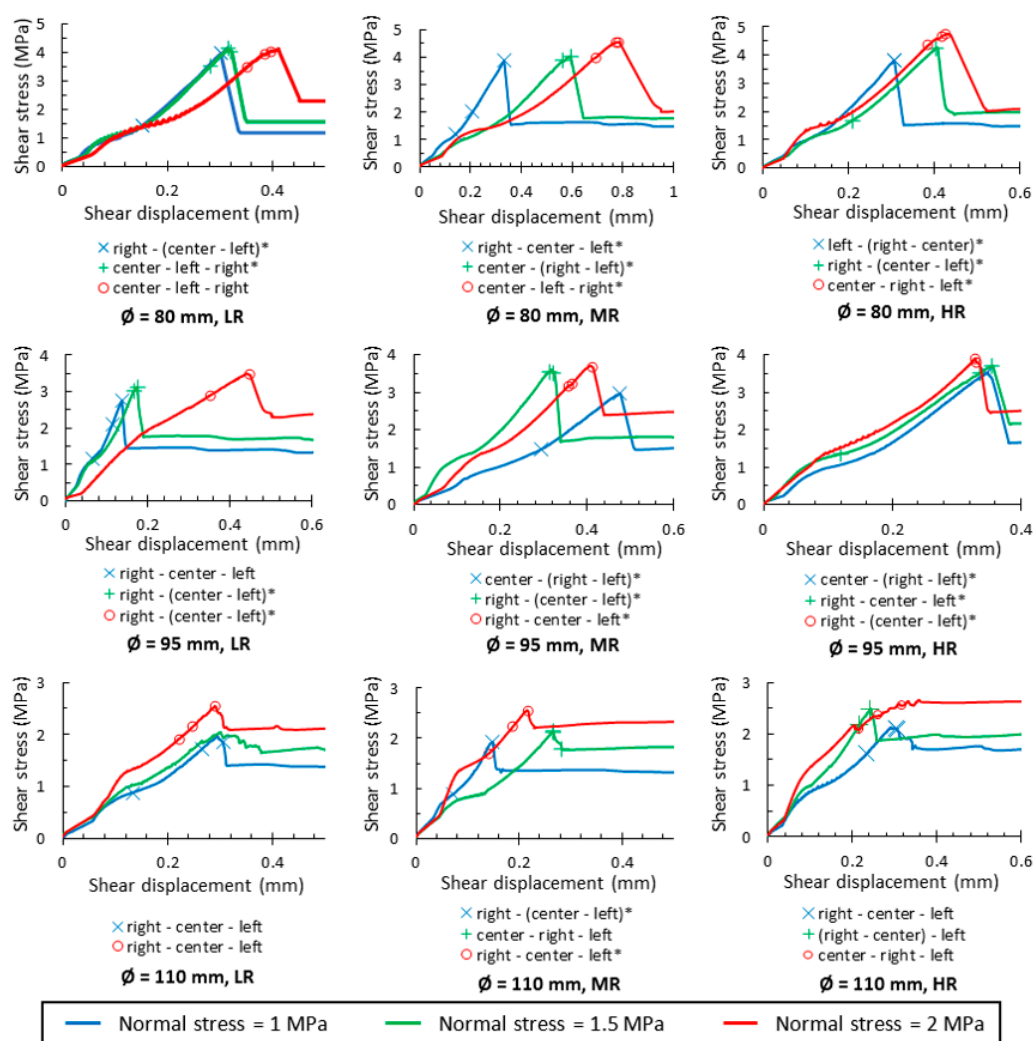


Figure 17. Crack initiation moments and the sequence of the cracks that lead to the failure of J&Br specimens containing a single joint with different sizes ($\varnothing = 80$ mm, $\varnothing = 95$ mm, $\varnothing = 110$ mm) and roughness (LR, MR, and HR) subjected to different normal stresses (1 MPa, 1.5 MPa, and 2 MPa).

5. Conclusions

A novel specimen preparation approach was applied to create rock-like specimens containing a non-persistent rough joint surrounded by intact material from all sides. Applying the casting method, the embedded joints are closed and interlocked, so their friction is mobilized once the specimens are subjected to the direct shear test condition. Unlike previously applied specimen preparation approaches, the proposed method enables the creation of embedded joints with different roughness levels along various directions.

In this study, the effects of three variables, namely rock bridge ratio, joint roughness, and applied normal stress on the shear behavior of rock-like specimens with non-persistent rough joints were experimentally investigated. The results of the experiments clearly demonstrated that all of the variables have impacts on the shear behavior of the specimens to different extents. The effect of rock bridge ratio and the normal stress on the shear strength of the specimens were found to be relatively more influential than that of joint roughness. The overall analysis of the peak shear displacement results revealed that the specimens with greater rock bridge ratios subjected to greater normal stresses undergo more shear displacement before the moment of failure. Moreover, the specimens with greater rock bridge ratios experience greater peak dilation when undergoing lower normal stresses.

The shear strength of the specimens with an open joint (Br specimens) and a single closed joint (J&Br specimens) were experimentally measured and the results were compared. The comparison revealed that the normal stress is partially applied to the jointed zone of the weakness planes, and the contribution of joint friction to the shear strength of the planes is not negligible. Moreover, the impact of joint roughness on the shear strength of J&Br specimens confirms that a fraction of normal load is applied to the embedded joint.

Three distinct phases of dilation were detected for specimens containing a non-persistent rough joint. The first phase demonstrates the dilation of the specimens before the failure point. A DIC analysis revealed that the dilation in this phase is mostly due to the rotation of the specimens as a result of the inevitable existing gap between the specimen holders of the direct shear test machine. In the second phase, dilation due to crack propagation and coalescence is followed by compression because of the closure of the enforced failure plane. Finally, the third phase of dilation complies with the dilation mechanism of a persistent rough joint. The walls of the enforced failure plane created after the failure of the specimens slide over each other in this phase.

The cracking process of the specimens containing a non-persistent rough joint was monitored with a camcorder. In most cases, the first crack was initiated at the axis of rotation and propagated to the circumference of the embedded joint and the last crack propagated from the other side of the joint circumference, eventually resulting in a rupture. Both cracks created a rough enforced shear plane with the embedded joint. It is important to note that the cracks that initiated and propagated before the final crack did not significantly alter the path of the shear stress–shear displacement curves. Most specimens with a smaller joint ($\varnothing = 80$ mm and $\varnothing = 95$ mm) were explosively broken whilst the cracks that initiated in the specimens with a wider embedded joint ($\varnothing = 110$ mm) smoothly propagated. The experimental results show that the joint roughness had no clear effect on the crack initiation moment and the sequence of the cracks.

Author Contributions: Conceptualization, S.F.; Formal analysis, S.F. and J.K.; Funding acquisition, J.-J.S.; Investigation, S.F., J.K. and J.-J.S.; Methodology, S.F. and J.-J.S.; Project administration, J.-J.S.; Supervision, J.-J.S.; Visualization, S.F. and J.K.; Writing—Original draft, S.F.; Writing—Review and editing, J.-J.S. and S.F. All authors have read and agreed to the published version of the manuscript.

Funding: This work was supported by a grant from the Human Resources Development program (No. 20204010600250) of the Korea Institute of Energy Technology Evaluation and Planning (KETEP), funded by the Ministry of Trade, Industry, and Energy of the Korean Government.

Institutional Review Board Statement: Not applicable.

Informed Consent Statement: Not applicable.

Acknowledgments: The authors are grateful to Jiwon Choi for her assistance during the experimental work at Rock Mechanics and Rock Engineering laboratory of Seoul National University.

Conflicts of Interest: The authors declare no conflict of interest.

References

1. Song, J.-J. Distribution-Free Method for Estimating Size Distribution and Volumetric Frequency of Rock Joints. *Int. J. Rock Mech. Min. Sci.* **2009**, *46*, 748–760. [\[CrossRef\]](#)
2. Deng, Q.; Zhang, P. Research on the Geometry of Shear Fracture Zones. *J. Geophys. Res. Solid Earth* **1984**, *89*, 5699–5710. [\[CrossRef\]](#)
3. Segall, P.; Pollard, D.D. Nucleation and Growth of Strike Slip Faults in Granite. *J. Geophys. Res. Solid Earth* **1983**, *88*, 555–568. [\[CrossRef\]](#)
4. Cheng, Y.; Wong, L.N.Y.; Zou, C. Experimental Study on the Formation of Faults from En-Echelon Fractures in Carrara Marble. *Eng. Geol.* **2015**, *195*, 312–326. [\[CrossRef\]](#)
5. Gehle, C.; Kutter, H.K. Breakage and Shear Behaviour of Intermittent Rock Joints. *Int. J. Rock Mech. Min. Sci.* **2003**, *40*, 687–700. [\[CrossRef\]](#)
6. Tuckey, Z.; Stead, D. Improvements to Field and Remote Sensing Methods for Mapping Discontinuity Persistence and Intact Rock Bridges in Rock Slopes. *Eng. Geol.* **2016**, *208*, 136–153. [\[CrossRef\]](#)
7. Barton, N. Shear Strength Criteria for Rock, Rock Joints, Rockfill and Rock Masses: Problems and Some Solutions. *J. Rock Mech. Geotech. Eng.* **2013**, *5*, 249–261. [\[CrossRef\]](#)
8. Barton, N. The Shear Strength of Rock and Rock Joints. *Int. J. Rock Mech. Min. Sci. Geomech. Abstr.* **1976**, *13*, 255–279. [\[CrossRef\]](#)
9. Barton, N. A Relationship between Joint Roughness and Joint Shear Strength. In Proceedings of the Rock Fracture International Symposium on Rock Mechanics, Nancy, France, 4–6 October 1971; pp. 1–8.
10. Barton, N.R. A Model Study of Rock-Joint Deformation. *Int. J. Rock Mech. Min. Sci. Geomech. Abstr.* **1972**, *9*, 579–582. [\[CrossRef\]](#)
11. Barton, N.; Choubey, V. The Shear Strength of Rock Joints in Theory and Practice. *Rock Mech.* **1977**, *10*, 1–54. [\[CrossRef\]](#)
12. Beer, G.; Poulsen, B.A. Efficient Numerical Modelling of Faulted Rock Using the Boundary Element Method. *Int. J. Rock Mech. Min. Sci. Geomech. Abstr.* **1994**, *31*, 485–506. [\[CrossRef\]](#)
13. Fox, D.J.; KaĹa, D.D.; Hsiung, S.M. Influence of Interface Roughness on Dynamic Shear Behavior in Jointed Rock. *Int. J. Rock Mech. Min. Sci.* **1998**, *35*, 923–940. [\[CrossRef\]](#)
14. Ladanyi, B.; Archambault, G. Simulation of Shear Behavior of a Jointed Rock Mass. In Proceedings of the the 11th U.S. Symposium on Rock Mechanics (USRMS), Berkeley, CA, USA, 1 January 1969.
15. Ge, Y.; Kulatilake, P.H.S.W.; Tang, H.; Xiong, C. Investigation of natural rock joint roughness. *Comput. Geotech.* **2014**, *55*, 290–305. [\[CrossRef\]](#)
16. Ge, Y.; Tang, H.; Ez Eldin, M.A.M.; Wang, L.; Wu, Q.; Xiong, C. Evolution process of natural rock joint roughness during direct shear tests. *Int. J. Geomech.* **2017**, *17*, E4016013. [\[CrossRef\]](#)
17. Grasselli, G.; Egger, P. Constitutive law for the shear strength of rock joints based on three-dimensional surface parameters. *Int. J. Rock Mech. Min. Sci.* **2003**, *40*, 25–40. [\[CrossRef\]](#)
18. Jiang, Y.; Li, B.; Tanabashi, Y. Estimating the relation between surface roughness and mechanical properties of rock joints. *Int. J. Rock Mech. Min. Sci.* **2006**, *43*, 837–846. [\[CrossRef\]](#)
19. Lee, H.S.; Park, Y.J.; Cho, T.F.; You, K.H. Influence of Asperity Degradation on the Mechanical Behavior of Rough Rock Joints under Cyclic Shear Loading. *Int. J. Rock Mech. Min. Sci.* **2001**, *38*, 967–980. [\[CrossRef\]](#)
20. Lee, Y.-K.; Park, J.-W.; Song, J.-J. Model for the Shear Behavior of Rock Joints under CNL and CNS Conditions. *Int. J. Rock Mech. Min. Sci.* **2014**, *70*, 252–263. [\[CrossRef\]](#)
21. Liu, R.; Lou, S.; Li, X.; Han, G.; Jiang, Y. Anisotropic Surface Roughness and Shear Behaviors of Rough-Walled Plaster Joints under Constant Normal Load and Constant Normal Stiffness Conditions. *J. Rock Mech. Geotech. Eng.* **2020**, *12*, 338–352. [\[CrossRef\]](#)
22. Maksimović, M. The Shear Strength Components of a Rough Rock Joint. *Int. J. Rock Mech. Min. Sci. Geomech. Abstr.* **1996**, *33*, 769–783. [\[CrossRef\]](#)
23. Park, J.-W.; Song, J.-J. Numerical Simulation of a Direct Shear Test on a Rock Joint Using a Bonded-Particle Model. *Int. J. Rock Mech. Min. Sci.* **2009**, *46*, 1315–1328. [\[CrossRef\]](#)
24. Patton, F.D. Multiple Modes of Shear Failure in Rock. In Proceedings of the 1st ISRM Congress, Lisbon, Portugal, 1 January 1966.
25. Prassetyo, S.H.; Gutierrez, M.; Barton, N. Nonlinear Shear Behavior of Rock Joints Using a Linearized Implementation of the Barton–Bandis Model. *J. Rock Mech. Geotech. Eng.* **2017**, *9*, 671–682. [\[CrossRef\]](#)
26. Seidel, J.P.; Haberfield, C.M. A Theoretical Model for Rock Joints Subjected to Constant Normal Stiffness Direct Shear. *Int. J. Rock Mech. Min. Sci.* **2002**, *39*, 539–553. [\[CrossRef\]](#)
27. Zhang, Q.; Li, X.; Bai, B.; Hu, H. The Shear Behavior of Sandstone Joints under Different Fluid and Temperature Conditions. *Eng. Geol.* **2019**, *257*, 105143. [\[CrossRef\]](#)
28. Zhao, J. Joint Surface Matching and Shear Strength Part A: Joint Matching Coefficient (JMC). *Int. J. Rock Mech. Min. Sci.* **1997**, *34*, 173–178. [\[CrossRef\]](#)
29. Zhao, J. Joint Surface Matching and Shear Strength Part B: JRC–JMC Shear Strength Criterion. *Int. J. Rock Mech. Min. Sci.* **1997**, *34*, 179–185. [\[CrossRef\]](#)

30. Ghazvinian, A.; Nikudel, M.R.; Sarfarazi, V. Effect of Rock Bridge Continuity and Area on Shear Behavior of Joints. In Proceedings of the International Society for Rock Mechanics and Rock Engineering, Lisbon, Portugal, 1 January 2007.
31. Savilahti, T.; Nordlund, E.; Stephansson, O. Shear Box Testing and Modeling of Joint Bridge. In Proceedings of the International Symposium on Rock Joints, Loen, Norway, 4 June 1990; pp. 295–300.
32. Shaunik, D.; Singh, M. Strength Behaviour of a Model Rock Intersected by Non-Persistent Joint. *J. Rock Mech. Geotech. Eng.* **2019**, *11*, 1243–1255. [[CrossRef](#)]
33. Wong, R.H.C.; Leung, W.L.; Wang, S.W. Shear Strength Studies on Rock-like Models Containing Arrayed Open Joints. In Proceedings of the the 38th U.S. Symposium on Rock Mechanics (USRMS), Washington, DC, USA, 1 January 2001.
34. Elmo, D.; Donati, D.; Stead, D. Challenges in the Characterisation of Intact Rock Bridges in Rock Slopes. *Eng. Geol.* **2018**, *245*, 81–96. [[CrossRef](#)]
35. Ghazvinian, A.; Sarfarazi, V.; Schubert, W.; Blumel, M. A Study of the Failure Mechanism of Planar Non-Persistent Open Joints Using PFC2D. *Rock Mech. Rock Eng.* **2012**, *45*, 677–693. [[CrossRef](#)]
36. Jiang, M.; Liu, J.; Crosta, G.B.; Li, T. DEM Analysis of the Effect of Joint Geometry on the Shear Behavior of Rocks. *Comptes Rendus Mécanique* **2017**, *345*, 779–796. [[CrossRef](#)]
37. Romer, C.; Ferentinou, M. Numerical Investigations of Rock Bridge Effect on Open Pit Slope Stability. *J. Rock Mech. Geotech. Eng.* **2019**, *11*, 1184–1200. [[CrossRef](#)]
38. Shang, J.; Zhao, Z.; Hu, J.; Handley, K. 3D Particle-Based DEM Investigation into the Shear Behaviour of Incipient Rock Joints with Various Geometries of Rock Bridges. *Rock Mech. Rock Eng.* **2018**, *51*, 3563–3584. [[CrossRef](#)]
39. Zhang, H.Q.; Zhao, Z.Y.; Tang, C.A.; Song, L. Numerical Study of Shear Behavior of Intermittent Rock Joints with Different Geometrical Parameters. *Int. J. Rock Mech. Min. Sci.* **2006**, *43*, 802–816. [[CrossRef](#)]
40. Fereshtenejad, S. Fundamental Study on Shear Behavior of Non-Persistent Joints. Ph.D. Thesis, Seoul National University, Seoul, Korea, 2020.
41. Muralha, J.; Grasselli, G.; Tatone, B.; Blümel, M.; Chrysanthakis, P.; Yujing, J. ISRM Suggested Method for Laboratory Determination of the Shear Strength of Rock Joints: Revised Version. In *The ISRM Suggested Methods for Rock Characterization, Testing and Monitoring: 2007–2014*; Ulusay, R., Ed.; Springer International Publishing: Cham, Switzerland, 2015; pp. 131–142. ISBN 978-3-319-07713-0.
42. Fereshtenejad, S.; Song, J.-J. Fundamental Study on Applicability of Powder-Based 3D Printer for Physical Modeling in Rock Mechanics. *Rock Mech. Rock Eng.* **2016**, *49*, 2065–2074. [[CrossRef](#)]
43. Ulusay, R. (Ed.) *The ISRM Suggested Methods for Rock Characterization, Testing and Monitoring: 2007–2014*; Springer International Publishing: Cham, Switzerland, 2015; ISBN 978-3-319-07712-3.
44. Tse, R.; Cruden, D.M. Estimating Joint Roughness Coefficients. *Int. J. Rock Mech. Min. Sci. Geomech. Abstr.* **1979**, *16*, 303–307. [[CrossRef](#)]
45. Lin, H.; Ding, X.; Yong, R.; Xu, W.; Du, S. Effect of Non-Persistent Joints Distribution on Shear Behavior. *Comptes Rendus Mécanique* **2019**, *347*, 477–489. [[CrossRef](#)]
46. MathWorks. Available online: <https://www.mathworks.com/matlabcentral/fileexchange/60817-surface-generator-artificial-randomly-rough-surfaces> (accessed on 7 May 2020).
47. Gao, Y.; Wong, L.N.Y. A Re-Examination of the Joint Roughness Coefficient (JRC) and Its Correlation with the Roughness Parameter Z_2 . In Proceedings of the 48th U.S. Rock Mechanics/Geomechanics Symposium, Minneapolis, MN, USA, 18 August 2014.
48. Fereshtenejad, S.; Song, J.-J. Applicability of Powder-Based 3D Printing Technology in Shear Behavior Analysis of Rock Mass Containing Non-Persistent Joints. *J. Struct. Geol.* **2021**, *143*, 104251. [[CrossRef](#)]
49. Lajtai, E.Z. Shear Strength of Weakness Planes in Rock. *Int. J. Rock Mech. Min. Sci. Geomech. Abstr.* **1969**, *6*, 499–515. [[CrossRef](#)]
50. Kulatilake, P.H.S.W.; Shreedharan, S.; Sherizadeh, T.; Shu, B.; Xing, Y.; He, P. Laboratory Estimation of Rock Joint Stiffness and Frictional Parameters. *Geotech. Geol. Eng.* **2016**, *34*, 1723–1735. [[CrossRef](#)]